Mesoporous Materials

DOI: 10.1002/ange.201303829

Flexible Mesoporous Photonic Resins with Tunable Chiral Nematic Structures**

*Mostofa K. Khan, Michael Giese, Marcus Yu, Joel A. Kelly, Wadood Y. Hamad, and Mark J. MacLachlan**

Coloration in nature plays essential roles in signaling, mimicry, or mate choice.[1,2] The striking color of a number of mussels, insect shells[3] (e.g., beetles, see Figure 1a), and bird feathers[4] arises from three-dimensional, hierarchically organized biomolecules.[5] These so-called photonic structures of nature are inspiring scientists to develop new materials with controllable structural color for applications in sensing and optoelectronics.[6–13] A powerful approach to photonic materials is to use templates that organize by molecular self-assembly.[14–17] Subsequent removal of the template releases a periodically mesoscopic structure with a photonic band gap. By changing the reaction conditions, the periodicity can be tuned and therefore the appearance and potential application of these materials can be controlled.[18–20]

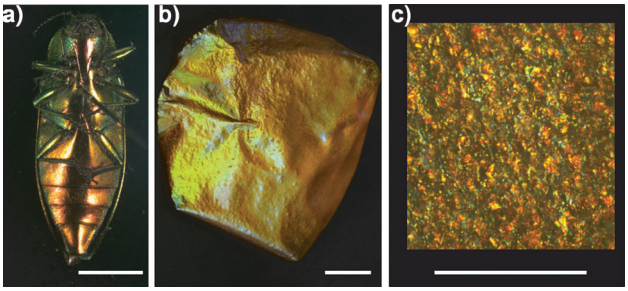

Figure 1. Photographs of a) a beetle (*buprestis fasciata*) native to British Columbia and b) the mesoporous resin films, showing the iridescent color that originates from the hierarchical structures. c) A magnified view of the surface of the mesoporous chiral nematic polymer. Scale bars from left to right: 5, 20, and 1 mm.

Cellulose nanocrystals (CNCs) derived by hydrolysis of bulk cellulose are known to form chiral nematic phases in aqueous solutions that dry to give iridescent films with chiral nematic organization.[21,22] Because of their fast self-assembly at low concentrations in water, CNCs offer an effective approach to developing structurally colored materials. Our group has explored the use of CNCs as a template for mesoporous inorganic solids with structural color (e.g., silica, titania).[23–25] Two significant drawbacks to the technological development of these freestanding films are their fragility and the static nature of their optical properties once the CNCs are removed, which we now seek to address by the development of a mesoporous plastic that captures the long-range chiral nematic and photonic properties of CNCs. Although CNCs have received considerable attention as a high-performance reinforcement in several (nonchiral nematic) polymeric systems,[26–31] no attempt has yet been made, to our knowledge, to develop a mesoporous plastic with chiral nematic organization.

Herein we report a mesoporous phenol–formaldehyde (PF) resin that exhibits the chiral nematic order of the CNCs, leading to colorful polymer films (Figure 1b,c). In comparison to other CNC-templated solids, the flexibility and responsive swelling behavior of the mesoporous films make them appealing for potential application in sensing and optics. This PF resin is the first of a family of plastic materials whose tunable properties might favorably combine chiral nematic coloration and mesoporosity.

Our approach to chiral nematic mesoporous polymers is shown in Scheme 1. An aqueous CNC dispersion (3.5%,

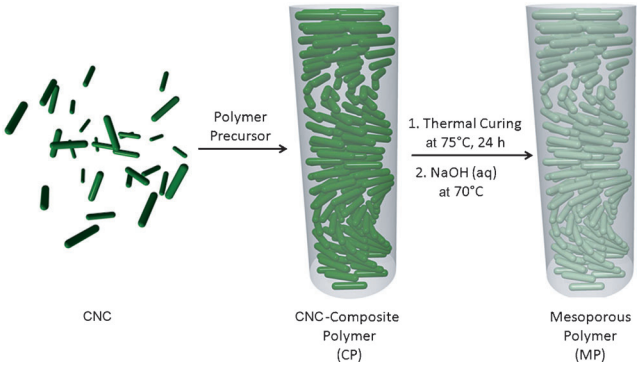

Scheme 1. Synthesis of the mesoporous chiral nematic PF resins. A CNC dispersion is mixed with an aqueous solution of the PF polymer precursor and cured to give chiral nematic composite films (CP). Alkaline treatment removes most of the CNC template, leading to highly iridescent, mesoporous photonic resins (MP) after supercritical drying.

[*] Dr. M. K. Khan, Dr. M. Giese, M. Yu, Dr. J. A. Kelly, Prof. M. J. MacLachlan
Department of Chemistry, University of British Columbia
2036 Main Mall, Vancouver, BC, V6T 1Z1 (Canada)
E-mail: mmaclach@chem.ubc.ca
Dr. W. Y. Hamad
FPInnovations
3800 Wesbrook Mall, Vancouver, BC, V6S 2L9 (Canada)

[**] Financial support for this work came from ArboraNano, NORAM Engineering & Constructors Ltd., and the German Academic Exchange Service (DAAD). We are grateful to FPInnovations for providing cellulose nanocrystals. The photograph of the beetle (Figure 1a) is courtesy of the Spencer Entomological Collection, Beaty Biodiversity Museum, UBC. Photographer: Don Griffiths.

Supporting information for this article is available on the WWW under http://dx.doi.org/10.1002/anie.201303829.

pH 2.4) derived by hydrolysis of wood pulp with sulfuric acid was mixed with an ethanolic solution of the PF precursor in water (35 wt%, pH 7). After drying under ambient conditions, colorful composite films were obtained. The films were then cured for 24 h at 75 °C to enhance crosslinking of the PF resins (composite polymer (CP) samples), resulting in slight shrinkage of the film and a blue shift in color of around 15 nm. Mesoporous, pliable resins with chiral nematic order can be obtained upon treatment of the composite with aqueous NaOH solution at 70 °C to remove the CNCs followed by supercritical drying of methanol-soaked films with CO_2 (mesoporous polymer (MP) samples).

Both the composites and the mesoporous polymer films were investigated with respect to their physical properties. The color of the composite films can be controlled by increasing the ratio of PF precursor to CNCs (**CP1**–**CP4**; resulting in a red shift) or the addition of salts such as NaCl (**CP1a**–**CP1d**; resulting in a blue shift; see Figure 2a). Both methods affect the helical pitch (P) of the chiral nematic CNC

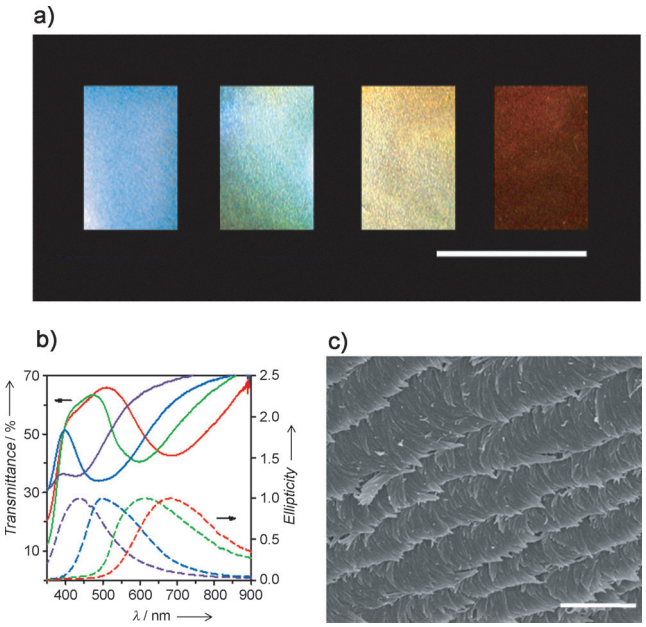

Figure 2. Characterization of the CNC–polymer composite films (**CP1a**–**CP1d**). a) The photograph shows the different colors of the composite films after curing, from right to left: **CP1a**, **CP1b**, **CP1c**, and **CP1d** (scale bar: 25 mm). All films are cured at 75 °C without addition of a curing agent. b) UV/Vis and CD spectra of the four samples (red: **CP1a**, green: **CP1b**, blue: **CP1c**, purple: **CP1d**) show their optical properties. c) SEM images support the left-handed orientation of the layers (scale bar: 1 μm).

phase, which, in combination with the average refractive index (n_{avg}) of the material, shifts the peak wavelength (λ_{max}) of light reflected by the chiral nematic structures at angle θ across the visible and near-IR spectral regions according to the following equation:[32]

$$\lambda_{max} = n_{avg} \cdot P \cdot \sin\theta \qquad (1)$$

By applying these methods, the maximum reflected wavelength at normal incidence of the composite samples (**CP1**–**CP4**) can be tuned from 430 to 685 nm (Figure 2b). To confirm that the observed reflection arises from the chiral nematic order of the polymer composites, samples were studied by polarized optical microscopy (POM), circular dichroism (CD) spectroscopy, and scanning electron microscopy (SEM). POM images (Figure S1 in the Supporting Information) show strong birefringence, which is a characteristic of chiral nematic organization. An intense signal in the CD spectra (Figure 2b) that corresponds to the reflection wavelength measured by UV/Vis spectroscopy confirms that the left-handed helical chiral nematic structure is embedded in the composites. SEM images (Figure 2c) also show a layered, twisted structure for the polymer composites that is consistent with a left-handed chiral nematic organization.

The curing step, which is necessary to form a robust composite film, gives highly iridescent, brittle films. Upon removal of the CNC template by treatment with NaOH, the mechanical properties change significantly. Samples **MP1a**–**MP1d** were obtained as flexible, iridescent films with blue-shifted reflection peak wavelengths (410 to 630 nm). Retention of chiral nematic order in the samples was confirmed by POM, CD spectroscopy, and SEM. The POM images show an obvious birefringence and a fingerprint structure indicative for a chiral nematic material (Figure 3a). The CD spectra (Figure 3b) show intense signals with positive ellipticity and SEM images show the twisted layered structure of a left-handed chiral nematic organization of the mesoporous films (Figure 3c).

CNC removal from the composite films was verified by several techniques. As noted above, the films exhibit a blue shift of around 50 nm after treatment with base followed by supercritical drying. This blue shift is consistent with removal of CNCs from the material, as it results from both a decreased refractive index (owing to pore generation) and shrinkage that decreases the pitch. IR spectra and ^{13}C cross-polarization/magic angle spinning (CP/MAS) NMR spectra show a substantial removal of the CNCs (Figure S2 and S3) as signals for the cellulose are diminished relative to those of the resin. Although ^{13}C CP/MAS NMR spectroscopy is not a quantitative method, it gives an estimation of the amount of cellulose removed. NMR spectra of the composite and the mesoporous polymer films (Figure S3) were obtained under similar conditions and a comparison of the relative area of the peaks shows removal of around 85–90 % of the CNCs during the treatment with NaOH. In addition, powder X-ray diffraction analysis confirms the removal by a significant drop in the intensity of the reflection peaks assigned to CNCs relative to the composite films (Figure S4). This observation is attributed to removal of the CNCs combined with a loss of crystallinity in the remaining cellulose in the resin samples.

Following the removal of the CNCs and the subsequent removal of methanol by supercritical drying, N_2 adsorption measurements of the MP samples show that the resulting PF resins are mesoporous. While the composite films with CNCs do not show any porosity, after the removal of CNCs, the MP films show a significant Brunauer–Emmett–Teller (BET) surface area ranging from 310–365 $m^2 g^{-1}$ and a pore volume

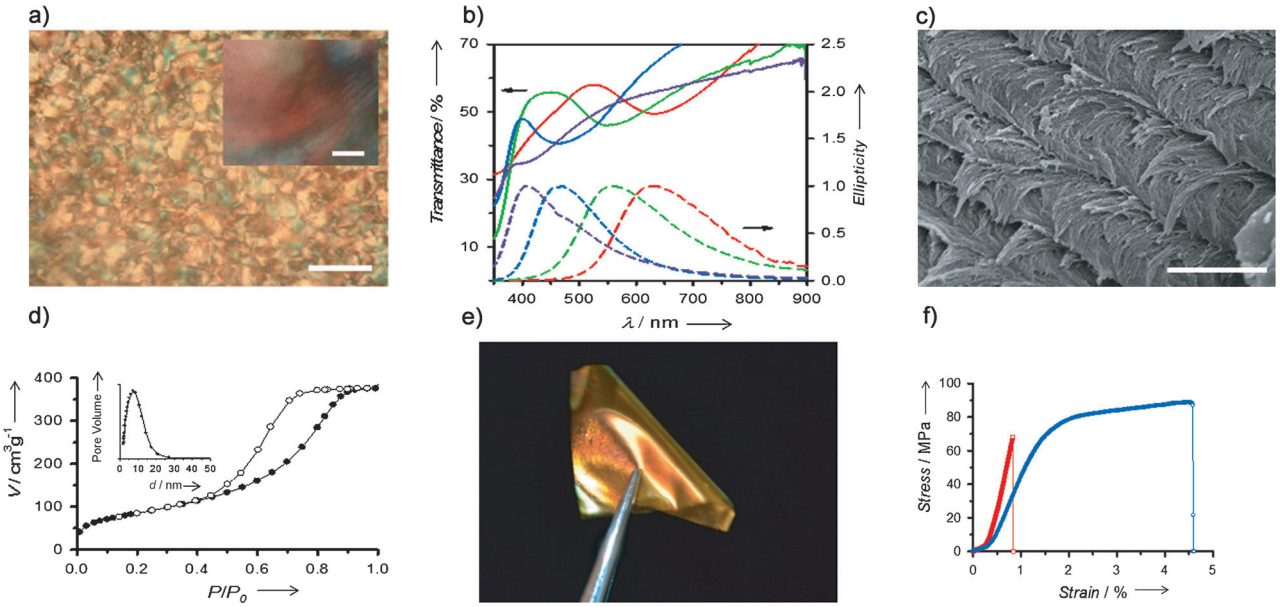

Figure 3. Characterization of the mesoporous polymer films (**MP1a**–**MP1d**) and illustration of the improved physical properties of the mesoporous polymer film **MP1a** with respect to the composite sample **CP1a**. a) POM images show a characteristic birefringence and fingerprint structure in regions of the samples (scale bars: main image 200 μm, inset 20 μm). b) Positive CD signals (red: **MP1a**, green: **MP1b**, blue: **MP1c**, purple: **MP1d**) and c) SEM image of the twisted layer structure of **MP1a** (as representative example, scale bar: 1 μm) support the left-handed chiral nematic organization of the polymer films. d) The significant BET surface area of 300–370 $m^2 g^{-1}$ and the calculation of the BJH pore-size diameters (see inset) are indicative for the removal of most of the CNCs (black circles: adsorption, white circles: desorption). e) The samples are pliable and can be bent without visible damage of the material (sample size around 1 cm^2). f) Stress-strain curve for a composite film (red) compared with that of the mesoporous plastic (blue).

of 0.5–0.7 $cm^3 g^{-1}$, depending on the composition of the sample (Figure 3d). The calculated Barrett–Joyner–Halenda (BJH) pore-size distributions are about 7 nm, which is close to the diameter of the individual CNCs that were removed from the composite.

Further evidence for CNC removal was obtained from measurements of the physical properties of the films before and after treatment. While thermogravimetric analysis (TGA) shows decomposition starting at around 165 °C for the composite material, the base-treated samples are stable up to about 300 °C (Figure S5). This stability arises from the CNC removal and concomitant enhanced crosslinking of the resin. Moreover, while the cured CNC/PF composites are brittle, they are tough and highly flexible after removal of the CNCs (Figure 3e). Tensile stress–strain curves measured on a mesoporous, chiral nematic resin after drying of methanol-soaked films with supercritical CO_2 showed tensile strength of around 89 MPa and elongation of about 4.5% at break (Figure 3f), comparable to the mechanical properties of commercial PF resins.[33] In other words, we have maintained the mechanical/thermal performance of the polymer and added new functionalities: mesoporosity and chiral nematic organization.

These materials exhibit unique photonic properties because of their combination of chiral nematic ordering, mesoporosity and responsive behavior. The films of **MP1a** appear brilliant red under a left-handed circular polarizer, and turn to dull brown upon observation through a right-handed circular polarizer (Figure 4a). This dramatic difference, which can be easily observed under polarizers, demonstrates a potential application of these materials as a unique security feature for documents and banknotes.

Upon immersion in solvents of different polarities, the mesoporous polymers swell rapidly, resulting in a red shift of the reflection peak as the helical pitch lengthens. Soaking the films in anhydrous ethanol results in only a small color change (from ca. 415 to 440 nm). On the other hand, samples immersed in water and mixtures of ethanol/water show large, tunable color changes (Figure 4b) as the helical pitch changes as a result of swelling of the mesoporous structure. The swelling behavior likely originates from a highly porous structure, combined with a low PF resin crosslinking density and/or a coating of residual cellulose in the mesopores. Interestingly, the response is very fast (Figure 4c), occurring within seconds; this response is much faster than that of previously reported photonic hydrogels,[34] and shows a large response range (Figure 4d), supporting the potential applications of these materials in sensing applications. Furthermore, the response is reversible.

The systematic shift of the color upon swelling in mixtures of ethanol and water with varying ratios can be easily followed with the naked eye and demonstrates the general potential of the mesoporous chiral nematic plastics as unique optical sensors. One advantage of these materials is that the CD spectrum of the materials rather than the UV-visible spectrum can be used as a measure of concentrations, which means that colored impurities will not substantially interfere.

In conclusion, we have discovered a new type of chiral mesoporous photonic resin by using cellulose nanocrystals as a template. The combination of photonic properties (from the

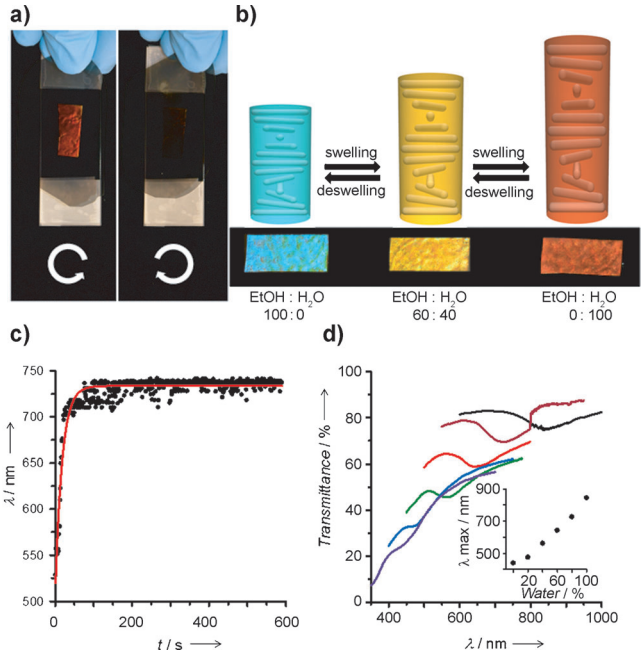

Figure 4. Demonstration of the potential application of the mesoporous photonic plastics (**MP1a** as representative example) in security features or optical sensors. a) The mesoporous sample appears bright red under a left-handed circular polarizer (a, left) while its color disappears under a right-handed polarizer (a, right). b) The swelling behavior of the mesoporous plastics in mixtures of water and ethanol (top: schematic illustration, bottom: photographs). Swelling of the material leads to a change in the helical pitch, affecting the color of the chiral nematic polymer films. c) The swelling kinetics of the samples in water shows a fast response of the material to solvent changes. The graph shows the rapid change in the reflection wavelength for the mesoporous polymer when a dry film is immersed in water. d) UV/Vis spectra show a systematic shift of the reflection signal of the chiral nematic resin during swelling in mixtures of water and ethanol (water content in solvent mixtures given in % (*v*/*v*); purple: 0, blue: 20, green: 40, orange: 60, dark red: 80, black: 100).

chiral nematic structure), mesoporosity, and flexibility available in these materials coupled with their scalable and straightforward synthesis makes these materials attractive for applications in sensing and optics, and as security features. Demonstrated with PF resins here, this process should be extendable to the diverse resin chemistry to construct a family of mesoporous, chiral nematic plastics.

Received: May 4, 2013
Published online: July 26, 2013

Keywords: cellulose · liquid crystalline template · mesoporous materials · polymers · resins

[1] S. Kinoshita, *Structural Colors in the Realm of Nature*, World Scientific, Singapore, **2008**.
[2] P. Vukusic, J. R. Sambles, *Nature* **2003**, *424*, 852 – 855.
[3] K. Michielsen, D. G. Stavenga, *J. R. Soc. Interface* **2008**, *5*, 85 – 94.
[4] M. D. Shawkey, A. M. Estes, L. M. Siefferman, G. E. Hill, *Proc. R. Soc. London Ser. B* **2003**, *270*, 1455 – 1460.
[5] A. E. Seago, P. Brady, J.-P. Vigneron, T. D. Schultz, *J. R. Soc. Interface* **2009**, *6*, S165 – S184.
[6] J. W. Galusha, L. R. Richey, M. R. Jorgensen, J. S. Gardner, M. H. Bartl, *J. Mater. Chem.* **2010**, *20*, 1277 – 1284.
[7] J. H. Holtz, S. A. Asher, *Nature* **1997**, *389*, 829 – 832.
[8] J. M. Jethmalani, W. T. Ford, *Chem. Mater.* **1996**, *8*, 2138 – 2146.
[9] S. H. Foulger, P. Jiang, A. Lattam, D. W. Smith Jr., J. Ballato, D. E. Dausch, S. Grego, B. R. Stoner, *Adv. Mater.* **2003**, *15*, 685 – 689.
[10] E. Yablonovitch, *Phys. Rev. Lett.* **1987**, *58*, 2059 – 2062.
[11] H. Míguez, S. M. Yang, N. Tétreault, G. A. Ozin, *Adv. Mater.* **2002**, *14*, 1805 – 1808.
[12] B. T. Holland, C. F. Blanford, A. Stein, *Science* **1998**, *281*, 538 – 540.
[13] Y. Y. Li, F. Cunin, J. R. Link, T. Gao, R. E. Betts, S. H. Reiver, V. Chin, S. N. Bhatia, M. J. Sailor, *Science* **2003**, *299*, 2045 – 2047.
[14] J. W. Steed, J. L. Atwood, *Supramolecular Chemistry*, Wiley, New York, **2000**.
[15] J.-M. Lehn, *Supramolecular Chemistry*: *Concepts and Perspectives*, VCH, New York, **1995**.
[16] D. G. Kurth, P. Lehmann, M. Schütte, *Proc. Natl. Acad. Sci. USA* **2000**, *97*, 5704 – 5707.
[17] R. F. Service, *Science* **2002**, *295*, 2398-2399.
[18] N. Huebsch, D. J. Mooney, *Nature* **2009**, *462*, 426 – 432.
[19] J. H. Moon, S. Yang, *Chem. Rev.* **2010**, *110*, 547 – 574.
[20] Y. Zhao, Z. Xie, H. Gu, C. Zhu, Z. Gu, *Chem. Soc. Rev.* **2012**, *41*, 3297 – 3317.
[21] J.-F. Revol, D. L. Godbout, D. G. Gray, US Patent 5,629,055, **1997**.
[22] J.-F. Revol, L. Godbout, D. G. Gray, *J. Pulp Pap. Sci.* **1998**, *24*, 146 – 149.
[23] K. E. Shopsowitz, H. Qi, W. Y. Hamad, M. J. MacLachlan, *Nature* **2010**, *468*, 422 – 425.
[24] Y. Shin, G. J. Exarhos, *Mater. Lett.* **2007**, *61*, 2594 – 2597.
[25] E. Dujardin, M. Blaseby, S. Mann, *J. Mater. Chem.* **2003**, *13*, 696 – 699.
[26] B. L. Peng, N. Dhar, H. L. Liu, K. C. Tam, *Can. J. Chem. Eng.* **2011**, *89*, 1191 – 1206.
[27] V. Favier, H. Chanzy, J. Y. Cavaille, *Macromolecules* **1995**, *28*, 6365 – 6367.
[28] M. A. S. Azizi Samir, F. Alloin, J.-Y. Sanchez, N. El Kissi, A. Dufresne, *Macromolecules* **2004**, *37*, 1386 – 1393.
[29] L. Petersson, I. Kvien, K. Oksman, *Compos. Sci. Technol.* **2007**, *67*, 2535 – 2544.
[30] M. Tatsumi, Y. Teramoto, Y. Nishio, *Biomacromolecules* **2012**, *13*, 1584 – 1591.
[31] G. Siqueira, J. Bras, A. Dufresne, *Polymers* **2010**, *2*, 728 – 765.
[32] H. L. DeVries, *Acta Crystallogr.* **1951**, *4*, 219 – 226.
[33] E. Lokensgard, *Industrial Plastics*: *Theory and Application*, *5th ed.*, Delmar, Clifton Park, **2010**. p. 500.
[34] M. Ben-Moshe, V. L. Alexeev, S. A. Asher, *Anal. Chem.* **2006**, *78*, 5149 – 5157.